



HAL
open science

**Size-based characterization of dendrigraft poly(L-lysine)
by free solution capillary electrophoresis using
polyelectrolyte multilayer coatings**

Sébastien Roca, Laurent Leclercq, Herve Cottet

► **To cite this version:**

Sébastien Roca, Laurent Leclercq, Herve Cottet. Size-based characterization of dendrigraft poly(L-lysine) by free solution capillary electrophoresis using polyelectrolyte multilayer coatings. *Journal of Chromatography A*, 2024, 1718, pp.464719. 10.1016/j.chroma.2024.464719 . hal-04560428

HAL Id: hal-04560428

<https://hal.umontpellier.fr/hal-04560428v1>

Submitted on 16 Oct 2024

HAL is a multi-disciplinary open access archive for the deposit and dissemination of scientific research documents, whether they are published or not. The documents may come from teaching and research institutions in France or abroad, or from public or private research centers.

L'archive ouverte pluridisciplinaire **HAL**, est destinée au dépôt et à la diffusion de documents scientifiques de niveau recherche, publiés ou non, émanant des établissements d'enseignement et de recherche français ou étrangers, des laboratoires publics ou privés.

1 **Size-based characterization of dendrigraft poly(L-lysine) by free solution**
2 **capillary electrophoresis using polyelectrolyte multilayer coatings**

3
4 Sébastien Roca¹, Laurent Leclercq^{1*}, Hervé Cottet^{1*}

5 ¹ IBMM, University of Montpellier, CNRS, ENSCM, Montpellier, France

6 * Corresponding authors: herve.cottet@umontpellier.fr ; laurent.leclercq@umontpellier.fr

7
8
9 **Abstract**

10 Dendrigraft poly(L-lysine) (DGL) constitutes a promising dendritic-like drug vehicle with high
11 biocompatibility and straightforward access via ring-opening polymerization of N-carboxyanhydride in
12 water. The characterization of the different generations of DGL is however challenging due to their
13 heterogeneity in molar mass and branching ratio. In this work, free solution capillary electrophoresis
14 was used to perform selective separation of the three first generations of DGL, and optimized conditions
15 were developed to maximize inter-generation resolution. To reduce solute adsorption on the capillary
16 wall, successive multiple ionic polymer layer (SMIL) coatings terminated with a polycation were
17 deposited onto the inner wall surface. PEGylated polycation was also used as the last layer for the control
18 of the electroosmotic flow (EOF), depending on the PEGylation degree and the methyl-polyethylene
19 glycol (mPEG) chain length. 1 kDa mPEG chains and low grafting densities were found to be the best
20 experimental conditions for a fine tuning of the EOF leading to high peak resolution. Molar mass
21 polydispersity and polydispersity in effective electrophoretic mobility were successfully determined for
22 the three first generations of DGL.

23
24 **Keywords:** Capillary electrophoresis, dendrigraft poly(L-lysine), polyelectrolyte multilayers,
25 PEGylation, EOF modulation.

26

27 **1. Introduction**

28 Capillary electrophoresis (CE) is an analytical technique that presents numerous benefits for
29 polymer and biopolymer analysis [1,2]. One limitation of the technique is analyte adsorption [1–6] that
30 decrease the separation efficiency and the overall analysis performances and repeatability. Adsorption
31 could be avoided or at least limited by the deposition of polyelectrolytes onto the capillary surface [7,8].

32 The implementation of Successive Multiple Ionic Polymer Layers (SMIL) capillary coating has
33 demonstrated effective reduction of adsorption and improved analytical efficiency in protein analysis
34 [9–23]. It was highlighted that the EOF remained consistently high when using fully ionized
35 polyelectrolytes (EOF mobility typically around ± 40 Tiselius Units (TU), with $1 \text{ TU} = 1 \times 10^{-9} \text{ m}^2 \text{ V}^{-1} \text{ s}^{-1}$)
36 [7]. This high EOF mobility resulted in short and repeatable analysis times but with possibly limited
37 resolutions (R_s) due to fast analysis. Since EOF is primarily influenced by both the nature of the last
38 polyelectrolyte layer and the composition of the background electrolyte (BGE) [21]. Modulating the
39 EOF can be achieved by using a weak polyelectrolyte as the final layer and/or by changing the pH and
40 ionic strength (I) of the BGE.

41 Due to its antifouling properties towards biological molecules [24–33], mPEG chains were
42 chemically linked to different polycations, which were subsequently employed as top layers in SMIL
43 capillary coatings [7]. It was demonstrated that the EOF was impacted when the mPEG chains length
44 exceeded the Debye length, the latter depending on the BGE ionic strength. Competitions between the
45 steric hindrance of mPEG chains and the shearing effect occurring in the Debye length zone, resulted
46 in a more or less pronounced hydrodynamic screening and decreased EOF value. The strong impact of
47 mPEG chains density was highlighted in that study, with EOF value decreasing from -45 TU for non-
48 PEGylated SMIL to only -5 TU for the same SMIL with the polycationic last layer modified with 5 kDa
49 mPEG chains. Such neutral coating behavior allowed higher peak separation efficiency and better peak
50 resolution (R_s) for protein separation [7].

51 A lot of applications can benefit from SMIL coatings and EOF modulation, especially
52 (bio)polymer characterization and protein characterization by CE/MS [34–39]. PEGylated SMILs could
53 pave the way to better CE-MS coupling, since high R_s and EOF control are key factors for efficient

54 analysis. Too high EOF value disturbs the formation of stable electrospray droplets and may lead to ion
55 suppression effects [40]. Various experiments concluded that near-zero EOF CE-MS experiments gave
56 excellent peak resolution, separation efficiency and allowed wider detection window (leading to better
57 mass spectra) [36–39].

58 In this work, we propose to use SMIL and PEGylated SMIL to characterize the three first
59 generations of dendrigraft poly(L-lysine) (DGL). DGL polycations are synthesized by successive ring-
60 opening polymerization of lysine protected N-carboxyanhydride in water, as described by Commeyras
61 et al. [41]. The first DGL generation (G_1) gives linear α -poly(L-lysine) (α -PLL) oligomers. The second
62 DGL generation (G_2) is a comb-like poly(L-lysine). The third generation of DGL (G_3) is a
63 hyperbranched poly-lysine. Up to five DGL generations can usually be synthesized, with increasing
64 branching ratio and molar mass. Their high solubility in water [41], their high structural stability upon
65 time [42], their easy chemical modification [43], their non-immunogenic behavior [44], their low
66 cytotoxicity [45] and their biocompatibility [46] make DGL, and dendrimers of lysine in general, of
67 great interest as novel drug delivery systems [47].

68 Regarding their size characterization, Dynamic Light Scattering (DLS) and Taylor Dispersion
69 Analysis (TDA) were used to determine DGL hydrodynamic radius [48,49]. An almost linear correlation
70 of the hydrodynamic radius with the generation number was observed, as expected for dendritic-like
71 structures. The impact of organic solvent on R_h measurement was studied by Yevlampieva et al.,
72 revealing high flexibility of DGL structure, compared to other dendrimers [49]. Size-Exclusion
73 Chromatography (SEC) coupled with multi-angle laser light scattering detection was used to determine
74 the molar mass distribution and polydispersity indexes [41,50]. CE and TDA were successfully used to
75 monitor surface functionalization of DGL [43]. DGL molar mass, hydrodynamic radius (R_h) and
76 effective charge (z_{eff}) are presented in Table 1. Colorimetric methods were used to determine of the
77 number of amino groups in DGL [48,51]. The overall DGL effective charge can be determined by
78 capillary isotachopheresis, leading to information about counter-ion condensation which was found to
79 dramatically increase with DGL generation number [52]. DGL characterization remains a complex task
80 due to multiple distributions in molar mass and branching ratio, and the relative sample polydispersities.

81 Among the analytical targets, the inter-generation purity is a key point since DGL (as other dendritic
82 structures) are synthesized step-by-step, from one generation to the other. Free solution CE analysis
83 appears to be well-suited to check inter-generation DGL purity due to its simplicity, low-cost and
84 relatively rapid and straightforward analysis without any sample preparation or filtration. The free
85 solution electrophoretic mobility is known to be independent of the molar mass for linear
86 polyelectrolytes above a certain molar mass (typically, 10^4 g/mol) [53], but depends on the branching
87 ratio, notably because the effective charge of the dendrimer changes with the counter-ion condensation
88 which is affected by the distance between adjacent charged monomers[52]. Collet et al. performed DGL
89 analysis up to the fifth generation by CE using a fused silica capillary, with however incomplete
90 separation between each generation [41]. G_1 analysis in free solution allows distinguishing seven peaks,
91 with poor peak resolution. Capillary gel electrophoresis (CGE) allows the separation of G_1 oligomers,
92 from 3 to 24 monomer units, but this method is more difficult to implement compared to free solution
93 CE and is time-consuming.

94 In the present work, we aim to improve the free solution CE separation of DGL G_1 to G_3 using PEGylated
95 SMIL and to determine their electrophoretic mobility dispersity and inter-generation purity.

96

97 **2. Experimental section**

98 **2.1. Chemicals and Materials.** Dendrigraft Poly(L-lysine) (DGL, G_1 , G_2 and G_3) were synthesized
99 in the laboratory according to [41]. 4-(2-hydroxyethyl)-1-piperazineethane sulfonic acid (HEPES,
100 99.5% purity), 2-Amino-2-(hydroxymethyl)-1,3-propanediol (Tris, > 99.9% purity), sodium nitrate
101 (99.0% purity) and penta-Lysine (> 55% purity) were purchased from Sigma-Aldrich (Saint-Quentin-
102 Fallavier, France). Sodium hydroxide (98 % purity) was purchased from Fluka (Saint-Quentin-Fallavier,
103 France). Sodium azide (99.5% purity) was purchased from Merck (Darmstadt, Germany). Acetic acid
104 (99.99% purity) was supplied by VWR Chemicals (Rosny-sous-Bois, France). Imidazole was purchased
105 from Acros Organics (Geel, Belgium). Orthophosphoric acid (85% content) was purchased from Prolabo
106 (Paris, France).

107 Methoxy-(polyethylene glycol)-succinimidyl carboxyl methyl ester (mPEG-NHS-SCM) of 1
108 kDa (PLS-215) and 5 kDa (PLS-213) average molar masses were purchased from Creative PEGWorks
109 (Durham, NC, USA). Poly(allylamine hydrochloride) (PAH, $M_w = 120\text{-}200$ kDa) was supplied by Alfa
110 Aesar (Kandel, Germany). Poly(diallyldimethylammonium chloride) (PDADMAC, $M_w = 450$ kDa)
111 were purchased from Sigma Aldrich (Saint-Quentin-Fallavier, France). Poly(sodium styrenesulfonate)
112 (PSS, $M_w = 70$ kDa) was purchased from Acros Organics (Geel, Belgium). Deionized water ($18\text{ M}\Omega\cdot\text{cm}^{-1}$)
113 delivered by a Synergy UV water purification system (Millipore, Fontenay-sous-Bois, France) was
114 used.

115 0.1 μm cut-off Durapore membrane filters were purchased from Millipore (Molsheim, France).
116 Dialysis tubings (cut-off: 1, 3.5, 8 and 12–14 kDa) were purchased from Spectrum Labs (San Francisco,
117 CA, USA).

118 PAH were PEGylated with either 1 kDa mPEG or 5 kDa mPEG, following EDC/NHS synthesis
119 protocol, as described in a previous paper [7]. For the 5 kDa mPEG polyelectrolyte modification, lower
120 grafting ratio than the targeted one was found due to possible steric hindrance of the long mPEG chains.
121 In contrast, a better control of the grafting ratio was obtained in the case of 1 kDa mPEGylation.
122 PEGylated PAH polycations were characterized by ^1H NMR (as given in supporting information in
123 Figure SII and SI2) and SEC-MALLS (Figure SI3). The main characteristics are gathered in Table 2.
124 More details about the experimental conditions for the characterization can be found in ref [7].
125 PEGylated PAH were named PAH-g-(mPEG $_x$) $_y$, where x corresponds to the mPEG length and y to the
126 measured PEGylated grafted ratio.

127

128 **2.2. SMIL coatings.** All SMIL capillary coatings were composed of a 4-layer (PDADMAC/PSS) $_2$
129 substructure terminated with either native or PEGylated PAH and were named (PDADMAC/PSS) $_2$ -
130 (PAH-g-(mPEG $_x$) $_y$) $_1$. Capillary coating procedure was performed according to [7,8,54]: flush at 930
131 mbar with NaOH 1 M solution for 10 min, followed by 5 min with pure water and 10 min with
132 construction buffer (HEPES/NaOH, 20 mM / 10 mM, pH 7.4). Next, polyelectrolyte solution (3 gL^{-1} of

133 PDADMAC or PSS in construction buffer) was flushed for 7 min, followed by a capillary rinsing with
134 the construction buffer (3 min). This step was repeated four times, starting with PDADMAC. For the
135 fifth layer coating, polyelectrolyte solution consisted of PAH (or its PEGylated derivative) dissolved at
136 3 gL^{-1} in the construction buffer, followed by a 3 min rinsing step with HEPES solution and 5 min wait.
137 Finally, the coated capillary was flushed with BGE for 10 min.

138

139 **2.3. Separation of dendrigraft poly(L-lysine) by capillary zone electrophoresis in free**
140 **solution.** Capillary zone electrophoresis experiments were performed on an Agilent 7100 CE piloted
141 by ChemStation software, using 58.5 or 88.5 cm capillary (50 and 80 cm of effective length, respectively,
142 $50 \text{ }\mu\text{m}$ capillary I.D. and $359 \text{ }\mu\text{m}$ capillary O.D.) and 125/250 mM Tris-phosphate BGE, pH 2.2 ($I =$
143 134.7 mM). Analyte (DGL G_1 , G_2 and G_3) were kept separately in BGE (at 2 gL^{-1}) in the freezer. BGE
144 was flushed for 3 min at 1 bar between each run. The separation voltage was +20 kV. DMF (0.001%
145 m/v in the BGE) and imidazole (0.001% m/v in BGE) were hydrodynamically injected as markers for 3
146 s at 30 mbar, followed by injection of DGL (2 or 0.5 gL^{-1} each in the BGE) for 4 s at 30 mbar. The
147 temperature of the cartridge was set at 25°C . Detection wavelengths were 214 and 200 nm.

148

149 **2.4. Polydispersity index (PDI) measurement.** Polydispersity index (*PDI*) gives information
150 about the dispersion of a given polymer distribution. *PDI* can be determined on molar mass distribution
151 using SEC, on hydrodynamic radius distribution using TDA or DLS [41], or on electrophoretic mobility
152 distribution using CE [55]. As described by Burchard in 1999 [56], polydispersity index relative to the
153 mass size distribution (PDI_M) can be expressed as (eq. 1):

154
$$PDI_M = \frac{M_w}{M_n} \quad (1)$$

155 where M_n and M_w are the number and weight average molar mass of the analyte, respectively.
156 Polydispersity index relative to the effective electrophoretic mobility distribution (PDI_μ) can be
157 expressed as (eq. 2) [56,57] :

158
$$PDI_\mu = \frac{\sigma_\mu^2}{\bar{\mu}_w^2} \quad (2)$$

159 with σ_{μ}^2 being the peak variance of the electropherogram modified by turning time x -scale into effective
160 electrophoretic mobility x -scale [58] and $\bar{\mu}_w^2$ being the average effective electrophoretic mobility of the
161 analyte.

162

163 **3. Results and discussion**

164 **3.1. Improving linear poly(L-lysine) oligomers separation in free solution CE by**

165 **EOF modulation.** In the first part of this work, we aimed to determine the best experimental
166 conditions for the analysis of the first generation of dendrigraft poly(L-lysine) (G_1) in free solution CE.
167 G_1 is a linear oligomeric poly(L-lysine). Experiments were carried out using Tris-phosphate buffer (125
168 mM / 250 mM, pH 2.2) as background electrolyte (BGE) and a 50 μm I.D. (O.D. = 359 μm) fused silica
169 capillary of 58.5 cm long (50 cm to the detector). Imidazole was used as the mobility marker. Effective
170 electrophoretic mobility of imidazole was +37.0 TU at +20 kV. In free solution CE, the electrophoretic
171 mobility of short oligomers can vary due to hydrodynamic coupling [59,60], but the main cause of the
172 selectivity in the present case is due to specific interaction between phosphate ions (H_2PO_4^-) and poly-
173 L-lysine [61,62].

174 As shown in Figure 1, the CE analysis of G_1 in a bare fused silica capillary at +20kV led to the
175 detection of broad distribution with low resolution between oligomers. The apparent mobility with the
176 fused silica capillary is $+5.56 \pm 0.06$ TU. The adsorption of poly(L-Lysine) onto the capillary wall is
177 limited in phosphate buffer at pH 2.2 due to almost neutral silica surface and probable interactions of
178 phosphate ions with poly(L-lysine) [62].

179 To improve this separation in free solution (i.e. without addition of gel or entangled polymer
180 solution in the BGE), it is possible to reduce the EOF magnitude, or even to reverse the EOF in a
181 controlled manner. By this way, the apparent mobility of the G_1 oligomers is decreased, which
182 consequently increases the apparent selectivity, and thus, the resolution, to the detriment of the analysis
183 time. As for G_1 separation, it is worth noting that the free solution electrophoretic effective mobility of
184 the poly(L-lysine) oligomers is changing with the molar mass due to two effects: interaction of
185 oligolysines with hydrogenophosphate ions and to a lower extent due to relaxation effect [62].

186 To improve G_1 separation, we used a 5-layers SMIL coating based on poly(diallyldimethylammonium
187 chloride) (PDADMAC) as the polycation, sodium poly(styrene sulfonate) (PSS) as the polyanion, and
188 a last layer containing variously PEGylated polyallylamine hydrochloride PAH-g-(mPEG)_x (where x is
189 the molar proportion of PEGylation on the PAH). 1 kDa and 5 kDa mPEG were used as grafting agents.
190 Synthesis and characterization of PEGylated PAH were realized following the protocol previously
191 described by Roca et al.[7]. As shown in Figure 1, 5kDa mPEG slightly reduces the EOF compared to
192 fused silica but do not reverse the EOF direction. This is due to the fact that the 5kDa mPEG chain
193 length (hydrodynamic diameter ~ 3.5 nm calculated from Mark-Houwink coefficients) [63] is much
194 higher than the Debye length (0.83 nm in the Tris-phosphate BGE), leading to important hydrodynamic
195 screening in the electrical double layer of the EOF generated by the cationic charges. Therefore, SMIL
196 terminated with a PAH-g-(mPEG_{5kDa})_x led to close to zero EOF, as displayed in Figure 2. The best EOF
197 regulation was obtained using PAH-g-(mPEG_{1kDa})_x, leading to a broad range of EOF mobility from -1.01
198 ± 0.11 TU for the 23.5% 1 kDa PEGylated PAH to -16.68 ± 0.10 TU in the case of unmodified PAH.
199 EOF mobility could be successfully regulated according to the 1 kDa mPEG proportion. A total of 10
200 peaks were detected for G_1 in about 20 min using SMIL coating terminated with PAH-g-(mPEG_{1kDa})_{0.065}
201 as the last layer. As for the G_1 separation, the unPEGylated PAH gives even higher resolution with an
202 analysis time of about 35 min.

203

204 **3.2. Optimize the separation of the three first generations of DGL.** EOF regulation
205 was applied to the analysis of DGL G_1 , G_2 and G_3 in free solution. This inter-generation separation is
206 essential to quantify the inter-generation purity. The separation between DGL generations is notably
207 driven by the drop in the effective charge per monomer with increasing generation number [52] which
208 can be explained by higher counter-ion condensation for higher branching ratios. The DGL
209 concentration was reduced from 2 gL⁻¹ to 0.5 gL⁻¹ to limit the electromigration dispersion (overloading
210 effect) and UV-detection was set at 200 nm for better sensitivity. G_1 , G_2 and G_3 were injected separately
211 to better visualize the co-migrations between DGL generations. As shown in Figure 3A, using a 58.5 cm
212 long bare fused silica capillary, G_1 to G_3 DGL were detected in less than 10 min with only partial
213 separation between generations, and only 4 peaks that can be distinguished for G_1 oligomers. Using

214 PAH-g-(mPEG_{1kDa})_{0.133} as the last layer gave better results with 7 distinguishable peaks for G₁ and better
215 separation between G₁ and G₂ and between G₂ and G₃. Finally, PAH-g-(mPEG_{1kDa})_{0.065} as the last layer
216 afforded the highest peak resolution, with 13 peaks detected for G₁ and improved peak separation
217 between G₁ and G₂. The three DGL generations were detected in 35 min (Figure 3A, upper trace).
218 UnPEGylated PAH was not used due to too high migration times.

219 Similar experiments were carried out on an 88.5 cm long capillary (80 cm to the detector) to further
220 increase the peak resolution (Figure 3B). 13 different peaks were detected using 13.3% and 6.5%
221 PEGylated PAH as last layer, with 2.38 and 2.53 peak resolution between the two highest peaks of G₁
222 (corresponding to a polymerization degree (*DP*) = 6 and 7), respectively, while other experiments
223 presented in Figure 3 never exceeded peak resolution of 1.50 (see Table SII). 88.5 cm long capillaries
224 were used to determine inter-generation DGL purity.

225

226 **3.3. Characterization of DGL polydispersity and inter-generational purity.** Peak
227 assignment of G₁ was performed on a 58.5 cm long fused silica capillary, coated with
228 (PDADMAC/PSS)₂-(PAH-g-(mPEG_{1kDa})_{0.033})₁. As shown in Figure 4, 13 peaks were detected in 26 min.
229 The peak assignment was done by spiking the G₁ sample with pentalysine (see Figure SI4).

230 Polydispersity index (*PDI*) of all three generations were calculated from the experimental data
231 obtained with an 88.5 cm long fused silica capillary, coated with (PDADMAC/PSS)₂-(PAH-g-
232 (mPEG_{1kDa})_{0.065})₁ SMIL. For G₁, *PDI* was measured according to two different ways, i.e. in terms of
233 molar mass polydispersity (*PDI_M*) and in terms of electrophoretic effective mobility polydispersity
234 (*PDI_μ*). Equations used to determine *PDI_M* and *PDI_μ* are given in section 2.3. The determination of *PDI_μ*
235 requires the transformation of the raw electropherogram (absorbance *A(t)* vs migration time (*t*)) into
236 effective electrophoretic mobility distribution (*P(μ) ~ A(t) × t*, see Figure 5A), following previously
237 described protocols [58]. More details about these transformations are provided in supporting
238 information (Figure SI5 and SI6). Both *PDI* values demonstrated relatively low polydispersity (Table
239 3).

240 In the case of G_2 and G_3 , PDI_M could not be determined since it is not possible to get the molar
241 mass (or DP) distributions. Indeed, to get the molar mass distributions, a bijective function between the
242 effective mobility and the molar mass would be required. Since the electrophoretic mobility of the
243 hyperbranched dendrimers are depending in a complex manner with the branching ratio, the effective
244 charge and indirectly with the molar mass, it is not possible to get such bijective function. In other words,
245 a given effective mobility can correspond to two (or more) DGL structures having different branching
246 ratios and different molar masses. Higher branching ratios are strongly lowering the effective charge per
247 monomer due to stronger counter-ion condensation [52]. This explains why the DGL effective mobility
248 decreased with DGL generation (higher branching ratio and lower effective charge per monomer). Only
249 PDI_μ values were calculated for G_2 and G_3 (Table 3). Since both G_2 and G_3 presented some
250 intergenerational impurities (G_1 in G_2 sample and both G_1 and G_2 in G_3 sample), PDI_μ was estimated on
251 the main peak (see Figure 5B and 5C). PDI_μ value decreased with increasing the generation number.
252 Beyond inter generation comparisons, PDI are of interest for the synthetic chemist to compare the batch-
253 to-batch reproducibility.

254 The inter-generational purity was calculated for G_2 and G_3 , using a (PDADMAC/PSS)₂-(PAH-
255 g-(mPEG_{1kDa})_{0.065})₁ coated capillary (Figure 6). Using CE-Val software to measure time-corrected peak
256 area, residual G_1 in G_2 was found to be about 4.3 ± 1.4 %, corresponding to 25 mgL^{-1} concentration of
257 G_1 in G_2 . The same way, residual G_1 and G_2 in G_3 were found to be about 56 mgL^{-1} (6.6 ± 1.0 %) and
258 97 mgL^{-1} (13.2 ± 2.8 %), respectively. The error bars given for the inter-generational purities were
259 evaluated based on the visual evaluation of the integration limits, as depicted by the red arrows in Figure
260 6.

261

262 **Conclusion**

263 In this paper, capillary coatings based on successive multiple ionic polymer layers (SMIL)
264 terminated with a PEGylated PAH layer were used to characterize the polydispersity and the inter-
265 generation purity of three dendrigraft poly(L-lysine)s generations. By changing the proportion of
266 PEGylation a controlled regulation of the EOF could be obtained to improve the intergeneration

267 separation. 13.3%, 6.5% and 3.3% 1kDa PEGylated polycations led to better resolution compared to
268 bare fused silica capillary. Finally, polydispersity indexes in mass and mobility were determined after
269 adequate transformations of the electropherograms into effective mobility distribution or *DP*
270 distributions.

271

272 **References**

- 273 [1] L. Leclercq, M. Morvan, J. Koch, C. Neusüß, H. Cottet, Modulation of the
274 electroosmotic mobility using polyelectrolyte multilayer coatings for protein analysis by
275 capillary electrophoresis, *Analytica Chimica Acta* 1057 (2019) 152–161.
276 <https://doi.org/10.1016/j.aca.2019.01.008>.
- 277 [2] M.G. Khaledi, *High-Performance Capillary Electrophoresis Theory, Techniques, and*
278 *Applications*, 1998.
- 279 [3] M.R. Schure, A.M. Lenhoff, Consequences of wall adsorption in capillary
280 electrophoresis: theory and simulation, *Anal. Chem.* 65 (1993) 3024–3037.
281 <https://doi.org/10.1021/ac00069a015>.
- 282 [4] S. Ghosal, Fluid mechanics of electroosmotic flow and its effect on band broadening
283 in capillary electrophoresis, *Electrophoresis* 25 (2004) 214–228.
284 <https://doi.org/10.1002/elps.200305745>.
- 285 [5] S. Ghosal, Electrokinetic flow and dispersion in capillary electrophoresis, *Annu. Rev.*
286 *Fluid Mech.* 38 (2006) 309–338. <https://doi.org/10.1146/annurev.fluid.38.050304.092053>.
- 287 [6] B. Gaš, M. Štědrý, E. Kenndler, Peak broadening in capillary zone electrophoresis,
288 *Electrophoresis* 18 (1997) 2123–2133. <https://doi.org/10.1002/elps.1150181203>.
- 289 [7] S. Roca, L. Leclercq, P. Gonzalez, L. Dhellemmes, L. Boiteau, G. Rydzek, H. Cottet,
290 Modifying last layer in polyelectrolyte multilayer coatings for capillary electrophoresis of
291 proteins, *J. Chromatogr. A* 1692 (2023) 463837.
292 <https://doi.org/10.1016/j.chroma.2023.463837>.
- 293 [8] L. Dhellemmes, L. Leclercq, A. Höchsmann, C. Neusüß, J.-P. Biron, S. Roca, H.
294 Cottet, Critical parameters for highly efficient and reproducible polyelectrolyte multilayer
295 coatings for protein separation by capillary electrophoresis, *J. Chromatogr. A* 1695 (2023)
296 463912. <https://doi.org/10.1016/j.chroma.2023.463912>.
- 297 [9] L. Leclercq, C. Renard, M. Martin, H. Cottet, Quantification of adsorption and
298 optimization of separation of proteins in capillary electrophoresis, *Anal. Chem.* 92 (2020)
299 10743–10750. <https://doi.org/10.1021/acs.analchem.0c02012>.
- 300 [10] L. Hajba, A. Guttman, Continuous-flow-based microfluidic systems for therapeutic
301 monoclonal antibody production and organ-on-a-chip drug testing, *J. Flow Chem.* 7 (2017)
302 118–123. <https://doi.org/10.1556/1846.2017.00014>.

- 303 [11] V. Dolník, Capillary electrophoresis of proteins 2005–2007, *Electrophoresis* 29 (2008)
304 143–156. <https://doi.org/10.1002/elps.200700584>.
- 305 [12] P.G. Righetti, C. Gelfi, B. Verzola, L. Castelletti, The state of the art of dynamic
306 coatings, *Electrophoresis* 22 (2001) 603–611. [https://doi.org/10.1002/1522-
307 2683\(200102\)22:4<603::AID-ELPS603>3.0.CO;2-N](https://doi.org/10.1002/1522-2683(200102)22:4<603::AID-ELPS603>3.0.CO;2-N).
- 308 [13] C.A. Lucy, A.M. MacDonald, M.D. Gulcev, Non-covalent capillary coatings for
309 protein separations in capillary electrophoresis, *J. Chromatogr A* 1184 (2008) 81–105.
310 <https://doi.org/10.1016/j.chroma.2007.10.114>.
- 311 [14] K.S. McMillan, A.G. McCluskey, A. Sorensen, M. Boyd, M. Zagnoni, Emulsion
312 technologies for multicellular tumour spheroid radiation assays, *Analyst* 141 (2016) 100–110.
313 <https://doi.org/10.1039/C5AN01382H>.
- 314 [15] S. Štěpánová, V. Kašička, Recent applications of capillary electromigration methods
315 to separation and analysis of proteins, *Analytica Chimica Acta* 933 (2016) 23–42.
316 <https://doi.org/10.1016/j.aca.2016.06.006>.
- 317 [16] S. Štěpánová, V. Kašička, Applications of capillary electromigration methods for
318 separation and analysis of proteins (2017–mid 2021) – A review, *Analytica Chimica Acta*
319 1209 (2022) 339447. <https://doi.org/10.1016/j.aca.2022.339447>.
- 320 [17] S. Bekri, L. Leclercq, H. Cottet, Polyelectrolyte multilayer coatings for the separation
321 of proteins by capillary electrophoresis: Influence of polyelectrolyte nature and multilayer
322 crosslinking, *J. Chromatogr. A* 1399 (2015) 80–87.
323 <https://doi.org/10.1016/j.chroma.2015.04.033>.
- 324 [18] A. Pallotta, I. Clarot, J. Beurton, B. Creusot, T. Chaigneau, A. Tu, P. Lavalley, A.
325 Boudier, Analytical strategy for studying the formation and stability of multilayered films
326 containing gold nanoparticles, *Anal. Bioanal. Chem.* 413 (2021) 1473–1483.
327 <https://doi.org/10.1007/s00216-020-03113-6>.
- 328 [19] L. Villemet, A. Cuchet, C. Desvignes, C.E. Sängler–van de Griend, Protein mapping of
329 peanut extract with capillary electrophoresis, *Electrophoresis* 43 (2022) 1027–1034.
330 <https://doi.org/10.1002/elps.202100004>.
- 331 [20] M. Horká, J. Šalplachta, P. Karásek, M. Roth, Sensitive identification of milk protein
332 allergens using on-line combination of transient isotachopheresis/micellar electrokinetic
333 chromatography and capillary isoelectric focusing in fused silica capillary with roughened
334 part, *Food Chem.* 377 (2022) 131986. <https://doi.org/10.1016/j.foodchem.2021.131986>.
- 335 [21] R. Konášová, M. Butnariu, V. Šolínová, V. Kašička, D. Koval, Covalent cationic
336 copolymer coatings allowing tunable electroosmotic flow for optimization of capillary
337 electrophoretic separations, *Analytica Chimica Acta* 1178 (2021) 338789.
338 <https://doi.org/10.1016/j.aca.2021.338789>.
- 339 [22] V. Šolínová, P. Tůma, M. Butnariu, V. Kašička, D. Koval, Covalent anionic
340 copolymer coatings with tunable electroosmotic flow for optimization of capillary
341 electrophoretic separations, *Electrophoresis* 43 (2022) 1953–1962.
342 <https://doi.org/10.1002/elps.202200130>.

- 343 [23] G.W. Somsen, R. Haselberg, K. Michalikova, E. Domínguez-Vega, Middle-Up
344 Characterization of the monoclonal antibody infliximab by capillary zone electrophoresis–
345 mass spectrometry, LCGC Europe-03-01-2019, Volume 32, Issue 3 (2019).
- 346 [24] M. Hedayati, D.F. Marruecos, D. Krapf, J.L. Kaar, M.J. Kipper, Protein adsorption
347 measurements on low fouling and ultralow fouling surfaces: A critical comparison of surface
348 characterization techniques, *Acta Biomaterialia* 102 (2020) 169–180.
349 <https://doi.org/10.1016/j.actbio.2019.11.019>.
- 350 [25] C.-M. Xing, F.-N. Meng, M. Quan, K. Ding, Y. Dang, Y.-K. Gong, Quantitative
351 fabrication, performance optimization and comparison of PEG and zwitterionic polymer
352 antifouling coatings, *Acta Biomaterialia* 59 (2017) 129–138.
353 <https://doi.org/10.1016/j.actbio.2017.06.034>.
- 354 [26] C. Zhang, J. Yuan, J. Lu, Y. Hou, W. Xiong, H. Lu, From neutral to zwitterionic
355 poly(α -amino acid) nonfouling surfaces: Effects of helical conformation and anchoring
356 orientation, *Biomater.* 178 (2018) 728–737.
357 <https://doi.org/10.1016/j.biomaterials.2018.01.052>.
- 358 [27] B.L. Leigh, E. Cheng, L. Xu, A. Derk, M.R. Hansen, C.A. Guymon, Antifouling
359 photograftable zwitterionic coatings on PDMS substrates, *Langmuir* 35 (2019) 1100–1110.
360 <https://doi.org/10.1021/acs.langmuir.8b00838>.
- 361 [28] X. Lin, P. Jain, K. Wu, D. Hong, H.-C. Hung, M.B. O’Kelly, B. Li, P. Zhang, Z.
362 Yuan, S. Jiang, Ultralow fouling and functionalizable surface chemistry based on zwitterionic
363 carboxybetaine random copolymers, *Langmuir* 35 (2019) 1544–1551.
364 <https://doi.org/10.1021/acs.langmuir.8b02540>.
- 365 [29] R.J. Smith, M.G. Moule, P. Sule, T. Smith, J.D. Cirillo, J.C. Grunlan, Polyelectrolyte
366 Multilayer Nanocoating Dramatically Reduces Bacterial Adhesion to Polyester Fabric, *ACS*
367 *Biomater. Sci. Eng.* 3 (2017) 1845–1852. <https://doi.org/10.1021/acsbiomaterials.7b00250>.
- 368 [30] F. Boulmedais, B. Frisch, O. Etienne, P. Lavalle, C. Picart, J. Ogier, J.-C. Voegel, P.
369 Schaaf, C. Egles, Polyelectrolyte multilayer films with pegylated polypeptides as a new type
370 of anti-microbial protection for biomaterials, *Biomater.* 25 (2004) 2003–2011.
371 <https://doi.org/10.1016/j.biomaterials.2003.08.039>.
- 372 [31] Z. Zhang, M. Moxey, A. Alswieleh, A.J. Morse, A.L. Lewis, M. Geoghegan, G.J.
373 Leggett, Effect of salt on phosphorylcholine-based zwitterionic polymer brushes, *Langmuir*
374 32 (2016) 5048–5057. <https://doi.org/10.1021/acs.langmuir.6b00763>.
- 375 [32] C. Wang, G.K. Such, A. Widjaya, H. Lomas, G. Stevens, F. Caruso, S.E. Kentish,
376 Click poly(ethylene glycol) multilayers on RO membranes: Fouling reduction and membrane
377 characterization, *J. Membrane Sci.* 409–410 (2012) 9–15.
378 <https://doi.org/10.1016/j.memsci.2012.02.049>.
- 379 [33] W.-L. Chen, R. Cordero, H. Tran, C.K. Ober, *50th Anniversary Perspective : Polymer*
380 *Brushes: Novel Surfaces for Future Materials*, *Macromolecules* 50 (2017) 4089–4113.
381 <https://doi.org/10.1021/acs.macromol.7b00450>.

- 382 [34] F.P. Gomes, J.R. Yates, Recent trends of capillary electrophoresis- mass spectrometry
383 in proteomics research, *Mass Spec. Rev.* 38 (2019) 445–460.
384 <https://doi.org/10.1002/mas.21599>.
- 385 [35] M. Pattky, C. Huhn, Advantages and limitations of a new cationic coating inducing a
386 slow electroosmotic flow for CE-MS peptide analysis: a comparative study with commercial
387 coatings, *Anal. Bioanal. Chem.* 405 (2013) 225–237. <https://doi.org/10.1007/s00216-012-6459-8>.
388
- 389 [36] Y. Zhao, L. Sun, M.D. Knierman, N.J. Dovichi, Fast separation and analysis of
390 reduced monoclonal antibodies with capillary zone electrophoresis coupled to mass
391 spectrometry, *Talanta* 148 (2016) 529–533. <https://doi.org/10.1016/j.talanta.2015.11.020>.
- 392 [37] R. Haselberg, T. De Vijlder, R. Heukers, M.J. Smit, E.P. Romijn, G.W. Somsen, E.
393 Domínguez-Vega, Heterogeneity assessment of antibody-derived therapeutics at the intact
394 and middle-up level by low-flow sheathless capillary electrophoresis-mass spectrometry,
395 *Analytica Chimica Acta* 1044 (2018) 181–190. <https://doi.org/10.1016/j.aca.2018.08.024>.
- 396 [38] M. Han, B.M. Rock, J.T. Pearson, D.A. Rock, Intact mass analysis of monoclonal
397 antibodies by capillary electrophoresis—mass spectrometry, *J. Chromatogr. B* 1011 (2016)
398 24–32. <https://doi.org/10.1016/j.jchromb.2015.12.045>.
- 399 [39] R. Haselberg, G.J. De Jong, G.W. Somsen, Low-flow sheathless capillary
400 electrophoresis—mass spectrometry for sensitive glycoform profiling of intact pharmaceutical
401 proteins, *Anal. Chem.* 85 (2013) 2289–2296. <https://doi.org/10.1021/ac303158f>.
- 402 [40] G. Jarvas, B. Fonslow, A. Guttman, Ionization efficiency, ion suppression and
403 detection sensitivity of CESI-MS, [https://sciex.com/tech-notes/ce/ionization-efficiency--ion-](https://sciex.com/tech-notes/ce/ionization-efficiency--ion-suppression-and-detection-sensitivity)
404 [suppression-and-detection-sensitivity](https://sciex.com/tech-notes/ce/ionization-efficiency--ion-suppression-and-detection-sensitivity).
- 405 [41] H. Collet, E. Souaid, H. Cottet, A. Deratani, L. Boiteau, G. Dessalces, J.-C. Rossi, A.
406 Commeyras, R. Pascal, An expeditious multigram-scale synthesis of lysine dendrigraft (DGL)
407 polymers by aqueous *N*-carboxyanhydride polycondensation, *Chem. Eur. J.* 16 (2010) 2309–
408 2316. <https://doi.org/10.1002/chem.200901734>.
- 409 [42] G. Coussot, T. Moreau, C. Faye, F. Vigier, M. Baqué, A. Le Postollec, S. Incerti, M.
410 Dobrijevic, O. Vandenabeele-Trambouze, Biochip-based instruments development for space
411 exploration: influence of the antibody immobilization process on the biochip resistance to
412 freeze-drying, temperature shifts and cosmic radiations, *Int. J. Astrobiol.* 16 (2017) 190–199.
413 <https://doi.org/10.1017/S1473550416000173>.
- 414 [43] T. Liu, F. Oukacine, H. Collet, A. Commeyras, L. Vial, H. Cottet, Monitoring surface
415 functionalization of dendrigraft poly-L-lysines via click chemistry by capillary electrophoresis
416 and Taylor dispersion analysis, *J. Chromatogr. A* 1273 (2013) 111–116.
417 <https://doi.org/10.1016/j.chroma.2012.11.074>.
- 418 [44] B. Romestand, J.-L. Rolland, A. Commeyras, G. Coussot, I. Desvignes, R. Pascal, O.
419 Vandenabeele-Trambouze, Dendrigraft poly-L-lysine: A non-immunogenic synthetic carrier
420 for antibody production, *Biomacromolecules* 11 (2010) 1169–1173.
421 <https://doi.org/10.1021/bm9012056>.

422 [45] J. Hofman, M. Buncek, R. Haluza, L. Streinz, M. Ledvina, P. Cigler, In vitro
423 transfection mediated by dendrigraft poly(L -lysines): The effect of structure and molecule
424 size, *Macromol. Biosci.* 13 (2013) 167–176. <https://doi.org/10.1002/mabi.201200303>.

425 [46] J. Chamieh, J.P. Biron, L. Cipelletti, H. Cottet, Monitoring biopolymer degradation by
426 Taylor dispersion analysis, *Biomacromolecules* 16 (2015) 3945–3951.
427 <https://doi.org/10.1021/acs.biomac.5b01260>.

428 [47] J.-P. Francoia, L. Vial, Everything you always wanted to know about poly- L -lysine
429 dendrigrafts (but were afraid to ask), *Chem. Eur. J.* 24 (2018) 2806–2814.
430 <https://doi.org/10.1002/chem.201704147>.

431 [48] H. Cottet, M. Martin, A. Papillaud, E. Souaïd, H. Collet, A. Commeyras,
432 Determination of dendrigraft poly- L -Lysine diffusion coefficients by Taylor dispersion
433 analysis, *Biomacromolecules* 8 (2007) 3235–3243. <https://doi.org/10.1021/bm070268j>.

434 [49] N. Yevlampieva, A. Dobrodumov, O. Nazarova, O. Okatova, H. Cottet,
435 Hydrodynamic behavior of dendrigraft polylysines in water and dimethylformamide,
436 *polymers* 4 (2012) 20–31. <https://doi.org/10.3390/polym4010020>.

437 [50] B. Maret, A. Crépet, C. Faye, L. Garrelly, C. Ladavière, Molar-mass analysis of
438 dendrigraft poly(L -lysine) (DGL) polyelectrolytes by SEC-MALLS: The “Cornerstone”
439 refractive index increment, *Macromol. Chem. Phys.* 216 (2015) 95–105.
440 <https://doi.org/10.1002/macp.201400400>.

441 [51] G. Coussot, E. Nicol, A. Commeyras, I. Desvignes, R. Pascal, O. Vandenabeele-
442 Trambouze, Colorimetric quantification of amino groups in linear and dendritic structures,
443 *Polym. Int.* 58 (2009) 511–518. <https://doi.org/10.1002/pi.2560>.

444 [52] A. Ibrahim, D. Koval, V. Kašička, C. Faye, H. Cottet, Effective charge determination
445 of dendrigraft poly- L -lysine by capillary isotachopheresis, *Macromolecules* 46 (2013) 533–
446 540. <https://doi.org/10.1021/ma302125f>.

447 [53] H. Cottet, P. Gareil, O. Theodoly, C.E. Williams, A semi-empirical approach to the
448 modeling of the electrophoretic mobility in free solution: Application to polystyrenesulfonates
449 of various sulfonation rates, *Electrophoresis* 21 (2000) 3529–3540.
450 [https://doi.org/10.1002/1522-2683\(200011\)21:17<3529::AID-ELPS3529>3.0.CO;2-2](https://doi.org/10.1002/1522-2683(200011)21:17<3529::AID-ELPS3529>3.0.CO;2-2).

451 [54] S. Roca, L. Dhellemmes, L. Leclercq, Polyelectrolyte multilayers in capillary
452 electrophoresis, *ChemPlusChem* 87 (2022). <https://doi.org/10.1002/cplu.202200028>.

453 [55] J.J. Thevarajah, A.T. Sutton, A.R. Maniego, E.G. Whitty, S. Harrisson, H. Cottet, P.
454 Castignolles, M. Gaborieau, Quantifying the heterogeneity of chemical structures in complex
455 charged polymers through the dispersity of their distributions of electrophoretic mobilities or
456 of compositions, *Anal. Chem.* 88 (2016) 1674–1681.
457 <https://doi.org/10.1021/acs.analchem.5b03672>.

458 [56] W. Burchard, Solution Properties of Branched Macromolecules, in: J. Roovers (Ed.),
459 *Branched Polymers II*, Springer Berlin Heidelberg, Berlin, Heidelberg, 1999: pp. 113–194.
460 https://doi.org/10.1007/3-540-49780-3_3.

461 [57] I. Desvignes, J. Chamieh, H. Cottet, Separation and characterization of highly charged
462 polyelectrolytes using free-solution capillary electrophoresis, *Polymers* 10 (2018) 1331.
463 <https://doi.org/10.3390/polym10121331>.

464 [58] J. Chamieh, M. Martin, H. Cottet, Quantitative Analysis in Capillary Electrophoresis:
465 Transformation of Raw Electropherograms into Continuous Distributions, *Anal. Chem.* 87
466 (2015) 1050–1057. <https://doi.org/10.1021/ac503789s>.

467 [59] H. Cottet, P. Gareil, From small charged molecules to oligomers: A semiempirical
468 approach to the modeling of actual mobility in free solution, *Electrophoresis* 21 (2000) 1493–
469 1504. [https://doi.org/10.1002/\(SICI\)1522-2683\(20000501\)21:8<1493::AID-
470 ELPS1493>3.0.CO;2-E](https://doi.org/10.1002/(SICI)1522-2683(20000501)21:8<1493::AID-ELPS1493>3.0.CO;2-E).

471 [60] K. Grass, U. Böhme, U. Scheler, H. Cottet, C. Holm, Importance of hydrodynamic
472 shielding for the dynamic behavior of short polyelectrolyte chains, *Phys. Rev. Lett.* 100
473 (2008) 096104. <https://doi.org/10.1103/PhysRevLett.100.096104>.

474 [61] S.A. Allison, C. Perrin, H. Cottet, Modeling the electrophoresis of oligolysines,
475 *Electrophoresis* 32 (2011) 2788–2796. <https://doi.org/10.1002/elps.201100006>.

476 [62] H. Wu, S.A. Allison, C. Perrin, H. Cottet, Modeling the electrophoresis of highly
477 charged peptides: Application to oligolysines, *J. Sep. Sci.* 35 (2012) 556–562.
478 <https://doi.org/10.1002/jssc.201100873>.

479 [63] E.A. Bekturov, Z.K. Bakauova, *Synthetic Water-soluble Polymers in Solution:*
480 *Polymeric Acids and Their Salts - Cationic Polyelectrolytes - Non-ionic Water-soluble*
481 *Polymers - Water-soluble Polymers*, Basel Heidelberg, 1986.

482

483

484

LIST OF CAPTIONS

485

486 **Figure 1 : Impact of the capillary coating on DGL G₁ analysis by CE in free solution.** Experimental
487 conditions: fused silica capillary of 58.5 cm total length (50 cm to detector) × 50 μm I.D. (359 μm O.D.).
488 Coating: none (fused silica) or (PDADMAC/PSS)₂ + a last layer as indicated in the figure. Coating
489 protocol: See section 2.1. BGE: Tris-phosphate buffer (125 / 250 mM), pH 2.2. Applied voltage: +20
490 kV. Hydrodynamic injection: 30 mbar, 4 s (0.27% of total capillary volume). Concentration of analytes:
491 I: Imidazole (0.001% m/v) used as mobility marker, G₁: DGL G₁ (2 gL⁻¹ in BGE). Temperature: 25°C.
492 UV detection: 214 nm.

493

494 **Figure 2 : Impact of the proportion of mPEG in the last layer of a 5 layers SMIL coating on**
495 **electroosmotic mobility.** Same experimental conditions as in Figure 1. Error bars were estimated as ±
496 one SD on *n* = 5 repetitions.

497

498 **Figure 3: Impact of the capillary coating for the separation of DGL G₁, G₂ and G₃ at pH 2.2 on a**
499 **58.5 cm (A) and 88.5 cm (B) long capillary by free solution CE.** Experimental conditions: fused silica
500 capillary of 58.5 and 88.5 cm total length (50 and 80 cm to detector) × 50 μm I.D. (359 μm O.D.).
501 Coating: none (fused silica) or (PDADMAC/PSS)₂ + last layer as indicated in the figure. Coating
502 protocol: See section 2.1. BGE: Tris-phosphate buffer (125 / 250 mM), pH 2.2. Applied voltage: +20
503 kV. Hydrodynamic injection: 30 mbar, 4 s (0.27% and 0.13% of total capillary volume, respectively).
504 Concentration of analytes: I: Imidazole (0.001% m/v) used as mobility marker, G₁: DGL G₁ (0.5 gL⁻¹),
505 G₂: DGL G₂ (0.5 gL⁻¹) and G₃: DGL G₃ (0.5 gL⁻¹) all in BGE. Temperature: 25°C. UV detection: 200
506 nm.

507

508 **Figure 4: Optimized DGL G₁ analysis at pH 2.2 using (PDADMAC/PSS)₂-(PAH-g-**
509 **(mPEG_{1kDa})_{0.033})₁ coated capillary by free solution CE.** Experimental conditions: fused silica capillary
510 of 58.5 total length (50 cm to detector) × 50 μm I.D. (359 μm O.D.). Coating protocol: See section 2.1.
511 BGE: Tris-phosphate buffer (125 / 250 mM), pH 2.2 Applied voltage: + 20 kV. Hydrodynamic injection:
512 30 mbar, 4 s (0.27% of total capillary volume). Concentration of analytes: G₁: DGL G₁ (0.5 gL⁻¹ in
513 BGE). Temperature: 25°C. UV detection: 200 nm.

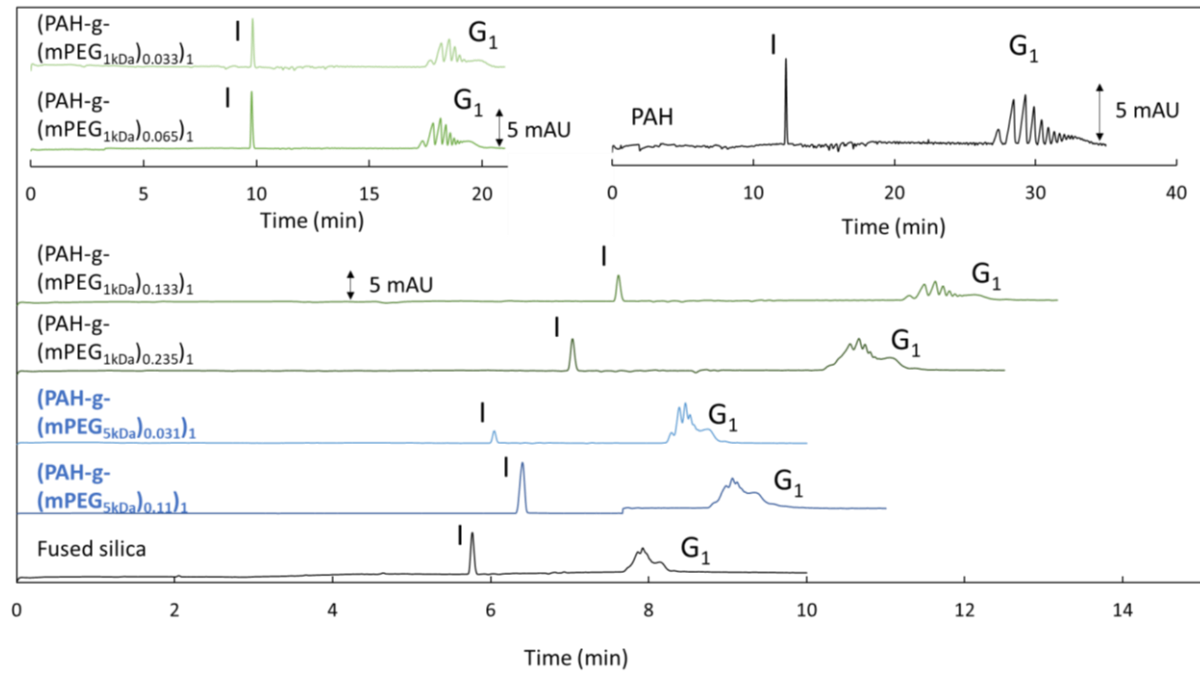
514

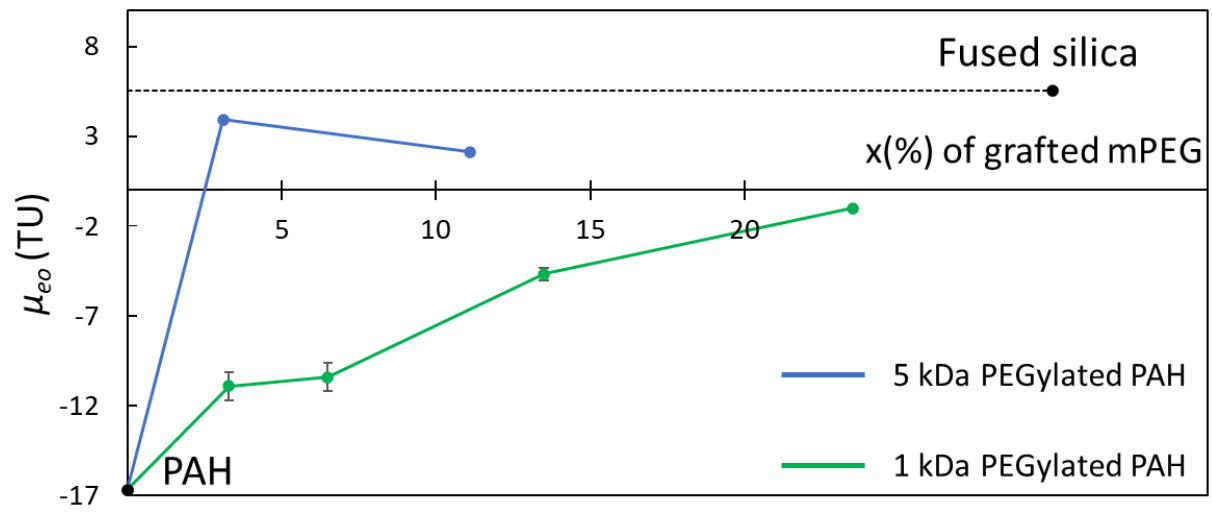
515 **Figure 5: Determination of *PDI_{M-1}* and *PDI_μ* for G₁ (A), G₂ (B) and G₃ (C) using**
516 **(PDADMAC/PSS)₂-(PAH-g-(mPEG_{1kDa})_{0.065})₁ coated capillary by CE in free solution.** Experimental
517 conditions: fused silica capillary of 88.5 total length (80 cm to detector) × 50 μm I.D. (359 μm O.D.).
518 Coating protocol: See section 2.1. BGE: Tris-phosphate buffer (125 / 250 mM), pH 2.2 Applied voltage:
519 + 20 kV. Hydrodynamic injection: 30 mbar, 4 s (0.13% of total capillary volume). Concentration of
520 analytes: DGL G₁, G₂ and G₃ (0.5 gL⁻¹ in BGE). Temperature: 25°C. UV detection: 200 nm.

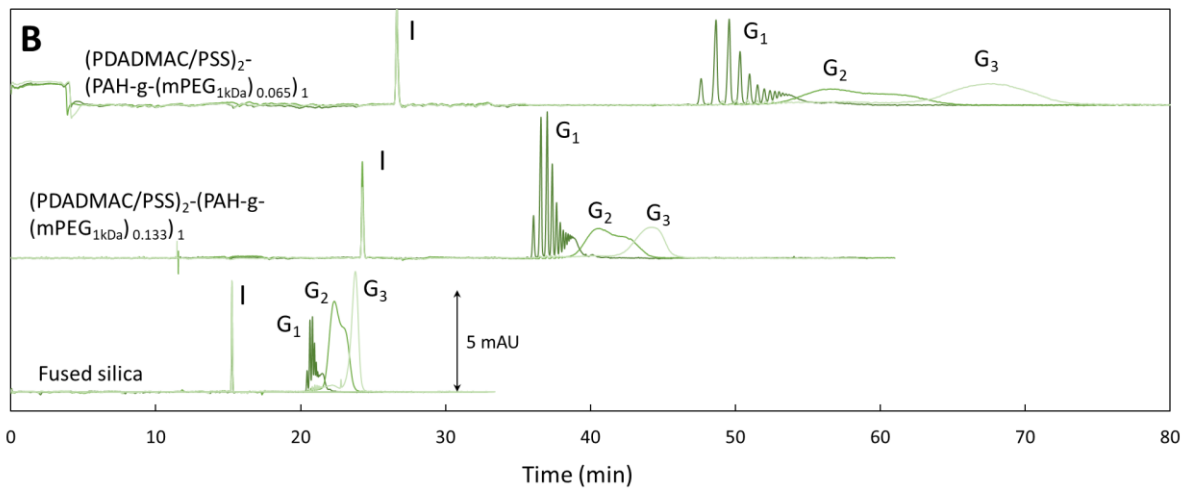
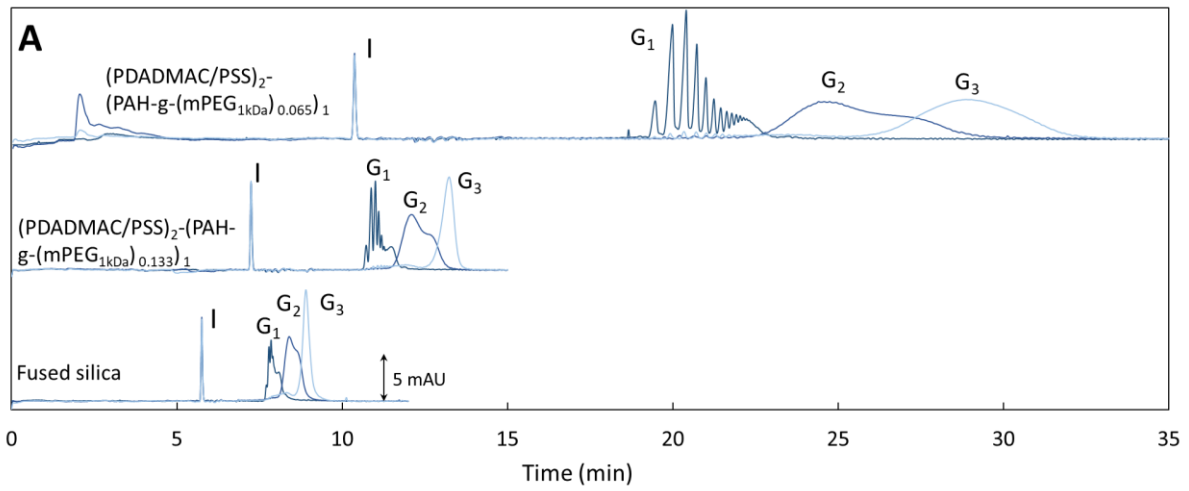
521

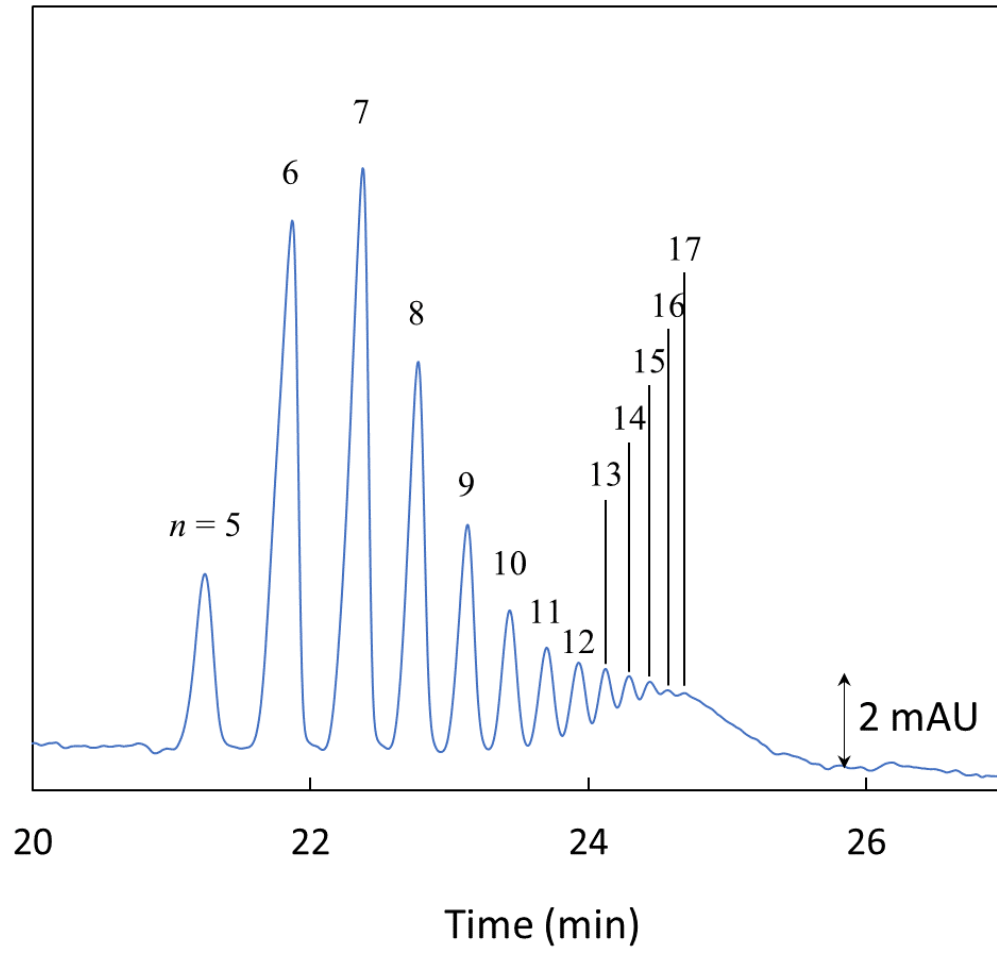
522 **Figure 6 : Determination of intergenerational impurity for G₂ and G₃ using (PDADMAC/PSS)₂-**
523 **(PAH-g-(mPEG_{1kDa})_{0.065})₁ coated capillary by CE in free solution.** Same experimental conditions as
524 in Figure 5. Baseline and integration limits used for intergeneration purity are displayed in the figure.
525 The middle ticks display the limits used to determine the average values given in the text. The red arrows
526 depict the integration limits used to estimate the errors on the inter-generation purities.

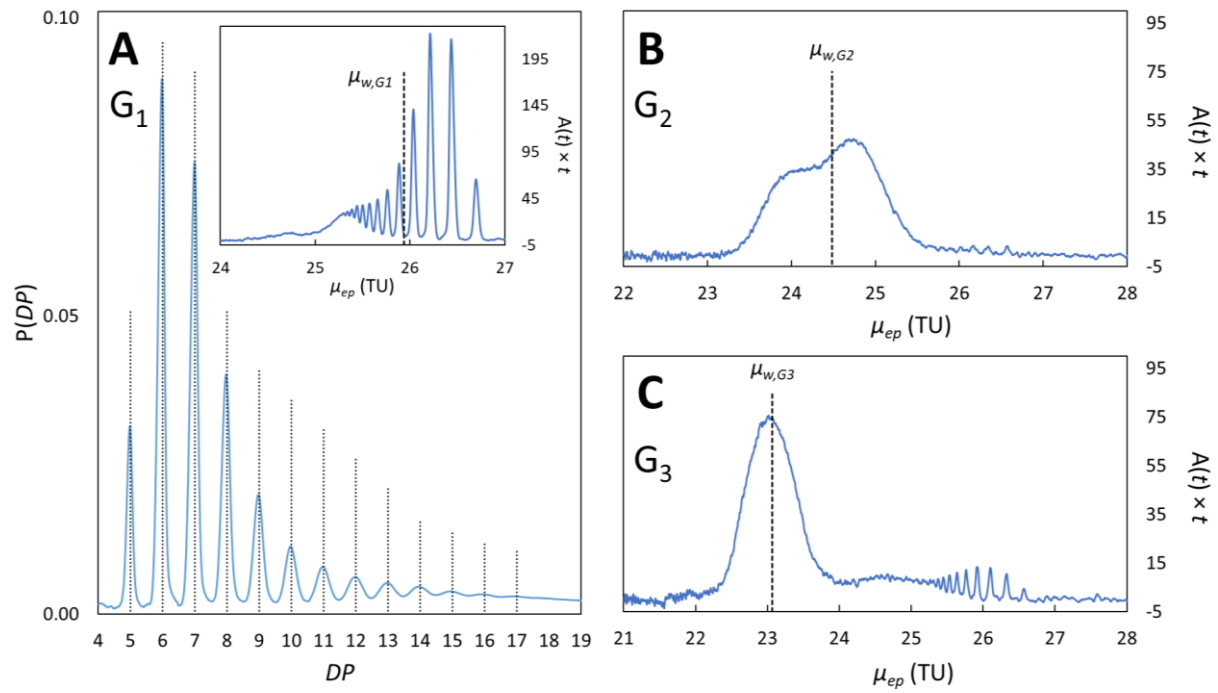
527











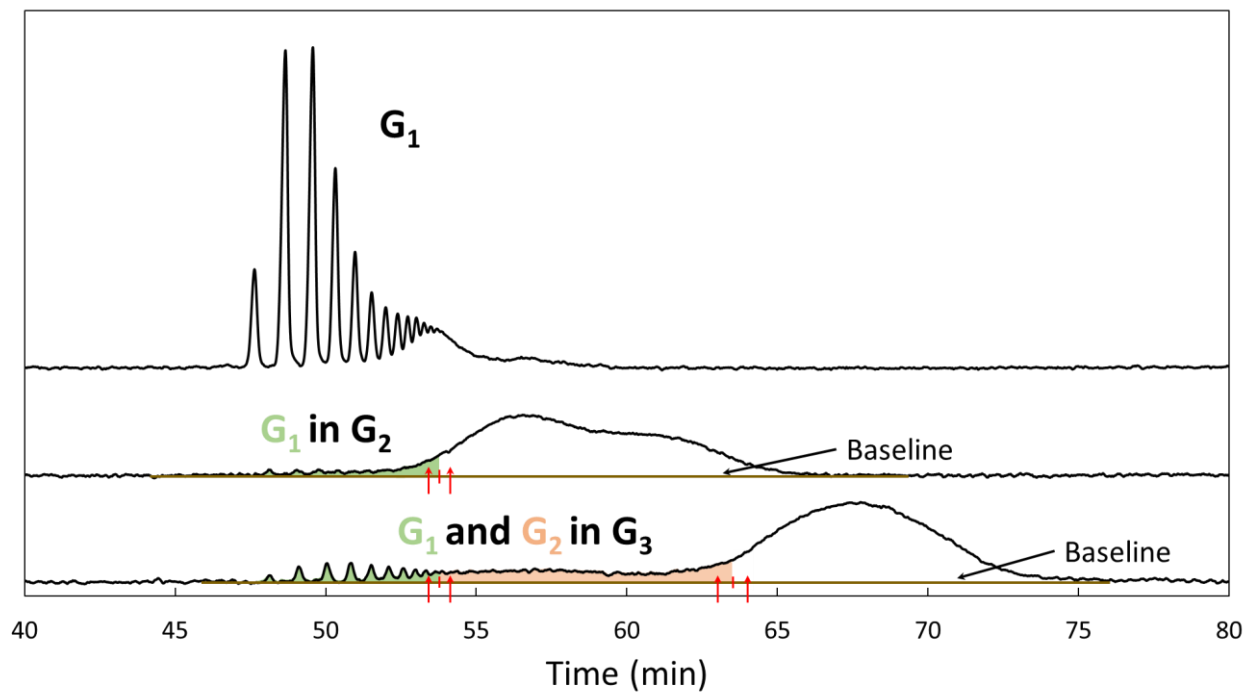


Table 1: Molar mass, hydrodynamic radius, and effective charge of the three first generations of DGL.

	G ₁	G ₂	G ₃
M_w (g mol ⁻¹) [43]	1 720	11 800	32 100
DP_n [41]	8	48	123
R_h (nm) [41]	1.03	1.96	3.06
Effective charge (z_{eff}) [50]	7	31	43

Table 2: Targeted and effective grafting ratio of the PEGylated poly(allylamine).

Polycation backbone	mPEG 1kDa				mPEG 5kDa	
	3%	6%	12%	20%	5%	20%
PAH	3.3 ^[a]	6.5 ^[a]	13.3 ^[a]	23.5 ^[a]	3.1 ^[b]	11.1 ^[b]

^[a] Grafting rates determined by ¹H NMR

^[b] Grafting rates determined by SEC-MALLS

Table 3: PDI_M and PDI_μ values for DGL G_1 , G_2 and G_3 . Error bars are \pm one SD ($n = 3$).

G_1					G_2			G_3		
DP_w	PDI_M	μ_w	σ_μ	PDI_μ (10^{-4})	μ_w	σ_μ	PDI_μ (10^{-4})	μ_w	σ_μ	PDI_μ (10^{-4})
7.66	1.09	26.05	0.49	3.61	24.39	0.50	4.28	23.28	0.33	1.97
± 0.04	± 0.05	± 0.09	± 0.02	± 0.3	± 0.1	± 0.02	± 0.36	± 0.18	± 0.01	± 0.18